AIP | Applied Physics Letters

A 2-terminal perovskite/silicon multijunction solar cell enabled by a silicon tunnel junction

Jonathan P. Mailoa, Colin D. Bailie, Eric C. Johlin, Eric T. Hoke, Austin J. Akey, William H. Nguyen, Michael D. McGehee, and Tonio Buonassisi

Citation: Applied Physics Letters **106**, 121105 (2015); doi: 10.1063/1.4914179
View online: http://dx.doi.org/10.1063/1.4914179
View Table of Contents: http://scitation.aip.org/content/aip/journal/apl/106/12?ver=pdfcov
Published by the AIP Publishing

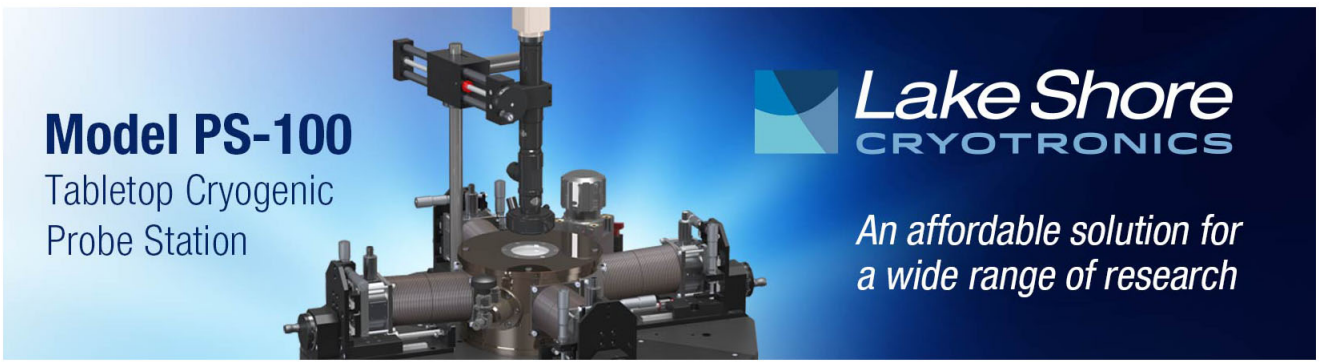

A 2-terminal perovskite/silicon multijunction solar cell enabled by a silicon tunnel junction

Jonathan P. Mailoa,[1,a),b)] Colin D. Bailie,[2,a)] Eric C. Johlin,[1] Eric T. Hoke,[2] Austin J. Akey,[1] William H. Nguyen,[2] Michael D. McGehee,[2,b)] and Tonio Buonassisi[1,b)]
[1]*Massachusetts Institute of Technology, Cambridge, Massachusetts 02139, USA*
[2]*Stanford University, Stanford, California 94305, USA*

(Received 4 February 2015; accepted 23 February 2015; published online 24 March 2015)

With the advent of efficient high-bandgap metal-halide perovskite photovoltaics, an opportunity exists to make perovskite/silicon tandem solar cells. We fabricate a monolithic tandem by developing a silicon-based interband tunnel junction that facilitates majority-carrier charge recombination between the perovskite and silicon sub-cells. We demonstrate a 1 cm^2 2-terminal monolithic perovskite/silicon multijunction solar cell with a V_{OC} as high as 1.65 V. We achieve a stable 13.7% power conversion efficiency with the perovskite as the current-limiting sub-cell, and identify key challenges for this device architecture to reach efficiencies over 25%. © *2015 AIP Publishing LLC*. [http://dx.doi.org/10.1063/1.4914179]

Solar-to-electricity conversion efficiency is the technical variable that most strongly influences silicon (Si) photovoltaic (PV) module costs.[1,2] The record efficiency of crystalline silicon (c-Si) single-junction PV devices has increased from 25% to 25.6% during the last fifteen years,[3,4] asymptotically approaching the 29.4% Auger-recombination-constrained Shockley-Queisser limit.[5] To make PV modules with higher efficiency than market-leading c-Si while leveraging existing c-Si manufacturing capacity, Si-based tandem approaches have been proposed.[6–10] The top sub-cell in a silicon-based tandem should have a band gap between 1.6 and 1.9 eV.[11] However, very few materials exhibit high open-circuit voltages (V_{OC}) within this band gap range. Recently, the methylammonium-lead-halide perovskite has demonstrated a rapid efficiency increase[12–16] with a V_{OC} of 1.15 V.[17] The methylammonium-lead-halide perovskite has a tunable band gap, ranging from 1.6 to 2.3 eV depending on halide composition,[18] though not all compositions are currently stable under illumination.[19] Methods to optically transmit longer-wavelength light through a top perovskite sub-cell in a mechanically stacked tandem configuration have been developed recently.[9,20]

A perovskite/Si multijunction solar cell may also be constructed *via* monolithic integration where a thin film perovskite sub-cell is deposited directly onto the c-Si sub-cell. Monolithic integration requires electrical coupling between sub-cells and transmission of infrared light to the bottom sub-cell. We use an interband tunnel junction[21] to facilitate electron tunneling from the electron-selective contact of the perovskite sub-cell into the *p*-type emitter of the Si sub-cell. This approach stands in contrast to the recombination layer used in other perovskite tandem systems[22] and is the one widely used in III-V[23] and micromorph (a-Si/μc-Si)[24] tandem solar cells. Unlike the tunnel junction in III-V multijunction solar cells, our tunnel junction is made of silicon with an indirect band gap, enabling electrical coupling with minimal parasitic absorption. The conduction-band alignment between Si and the perovskite sub-cell's electron-selective contact (TiO_2) enables bypassing the usage of a transparent conducting oxide (TCO) recombination layer, an alternative option with greater parasitic absorption. In this work, we use the methylammonium-lead(II)-iodide perovskite ($CH_3NH_3PbI_3$), which has a 1.61 eV band gap.[25] Herein, we present the device design, fabrication, characterization, and loss analysis of monolithic perovskite/Si multijunction solar cells.

We develop a 2-terminal perovskite/Si multijunction architecture on an *n*-type Si solar cell (Figure 1(a)) with 1 cm^2

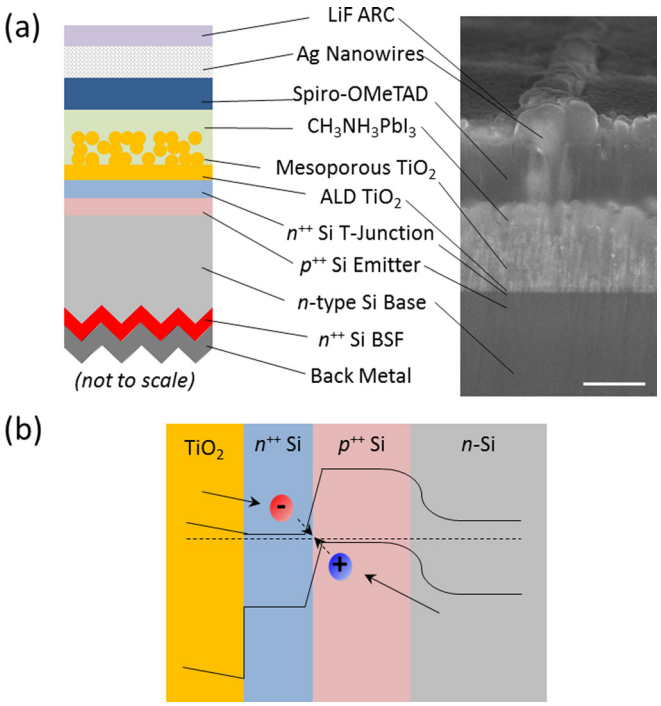

FIG. 1. (a) The device structure of a 2-terminal monolithically grown perovskite/Si multijunction solar cell with an *n*-type Si base. The polished SEM image is taken at 45° tilt to show the Ag nanowire mesh (500 nm scale bar). (b) Band diagram of the perovskite/silicon cell interface showing the charge-transport mechanism around the Si tunnel junction.

[a)]J. P. Mailoa and C. D. Bailie contributed equally to this work
[b)]Authors to whom correspondence should be addressed. Electronic addresses: jpmailoa@alum.mit.edu; mmcgehee@stanford.edu; and buonassisi@mit.edu

area. We process an *n*-type Si sub-cell with planar top surface and full-area *p*-type emitter and *n*-type back surface field (BSF) using standard Si processing techniques.[26] A tunnel junction facilitates carrier recombination (holes from the *n*-type Si base passing through the *p*-type emitter and electrons from the perovskite layer passing through its TiO_2 electron transport layer, respectively, as shown in Figure 1(b)). We form an n^{++}/p^{++} tunnel junction by depositing heavily doped n^{++} hydrogenated amorphous silicon (a-Si:H) using plasma-enhanced chemical vapor deposition (PECVD).[26] The 30 nm-thick a-Si:H layer is subsequently annealed in N_2 ambient at 680 °C for 15 min to activate the dopants.[27] It is known that interdiffusion of dopant species during the device fabrication process (such as the dopant activation anneal) may degrade the tunnel junction conductivity. Accordingly, a 2–3 nm-thick intrinsic a-Si layer is inserted between the p^{++} emitter and the n^{++} amorphous Si layer during the PECVD process[26] to mitigate possible dopant interdiffusion.[28] After the dopant-activation anneal, the amorphous layers are partially crystallized as shown by transmission electron microscopy (TEM, Figure 2(a)). Using secondary ion mass spectrometry (SIMS), we show the dopant concentration on the n^{++}/p^{++} Si interface after the dopant activation anneal is 10^{19}–$10^{20}\,cm^{-3}$, which is suitable to form a high-quality interband tunnel junction (Figure 2(b)).[28]

The addition of the tunnel junction on top of the single-junction *n*-type solar cell slightly reduces the short-circuit current (J_{SC}), but the presence of the tunnel junction has a negligible effect on the series resistance (Figure S1) indicating proper operation of the tunnel juntion.[26] The slight reduction in J_{SC} is due to parasitic absorption at $\lambda < 500$ nm (Figure S2),[26] which does not affect tandem performance as this portion of the spectrum is absorbed in the perovskite cell before reaching the tunnel junction.

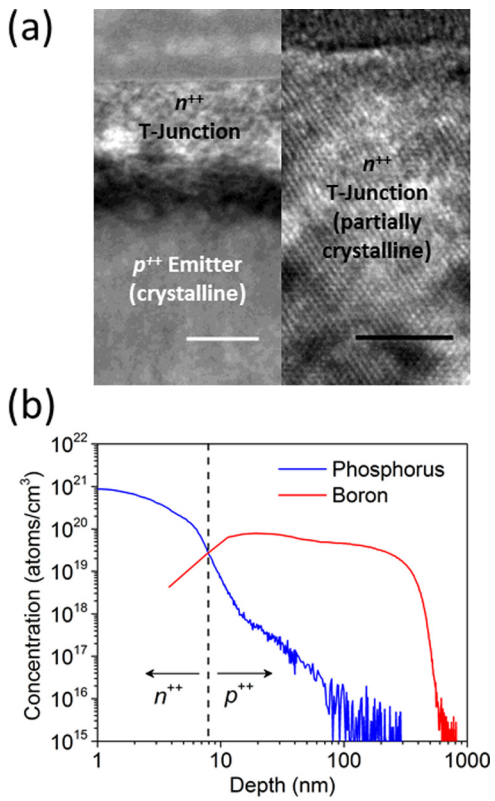

FIG. 2. (a) TEM image of the n^{++}/p^{++} silicon tunnel junction interface after the dopant activation annealing (left: 30 nm scale bar) and high-resolution TEM image of the n^{++} layer, showing the partially crystalline nature of this layer (right: 5 nm scale bar). (b) SIMS profile of the Si emitter and tunnel junction layer showing the sharp doping profile at the tunnel junction interface.

The efficiency of the planar single-junction Si cells is 13.8%. This efficiency is lower than commercial averages in part due to tandem design considerations. These intentional design considerations are: (1) No surface texturing for light trapping is applied because a planar front surface simplifies deposition of the perovskite; (2) No *p*-type front surface passivation scheme is applied on the emitter because the same technique cannot be implemented on the *n*-type portion of the tunnel junction. Other causes of lower efficiency are: (1) full-area BSF passivation only provides moderate passivation; (2) a front surface passivation scheme that can be decoupled from the tunnel junction formation needs to be developed; (3) dedicated clean furnaces for emitter formation and back surface passivation are necessary to make more efficient Si sub-cells.

We fabricate the monolithic perovskite/Si multijunction solar cell by depositing a perovskite sub-cell on top of the tunnel junction. We first metallize the back of our Si sub-cell, then deposit a 30 nm-thick TiO_2 layer on the planar n^{++} c-Si front surface using atomic layer deposition (ALD).[26] This TiO_2 layer is the *n*-type heterojunction for the perovskite sub-cell. It is known that TiO_2 is a good electron-selective contact for c-Si because of its conduction-band alignment,[29] which also eases electron transport from the TiO_2 layer into the n^{++} Si tunnel junction layer.[30,31] The thickness of this ALD TiO_2 layer can impact the optical transmission into the Si sub-cell (Figure S3),[26] and hence further thickness optimization is needed. The perovskite is deposited onto a mesoporous TiO_2 layer in a two-step conversion method.[15,26] An organic *p*-type heterojunction contact, spiro-OMeTAD, is deposited by spin-coating on top of the perovskite and is chemically doped with spiro-$(TSFI)_2$.[32] The top silver nanowire (AgNW) electrode is deposited using the procedure developed by Bailie *et al.*[9] AgNWs are sprayed from solution onto a plastic (PET) film, and then transferred from the PET to the spiro-OMeTAD layer via mechanical transfer through the application of pressure via a ball bearing. The silver nanowire electrode before transfer has a sheet resistance of 9 Ω/□ with a peak transmission of 89.5%. A 111-nm-thick lithium fluoride (LiF) anti-reflection layer is then deposited by thermal evaporation.

The *J-V* curve of our 2-terminal perovskite/Si multijunction solar cell under simulated AM1.5G illumination is shown in Figure 3(a). Due to the hysteresis often observed in metal-halide perovskite solar cells, it is important to be rigorous with *J-V* characterization.[33] We use a 5 s delay after each 100 mV voltage step before measuring the current in both scan directions. However, we still find hysteresis at this scan rate and that up to 30 s is required to reach a steady-state. This yields an overestimation of the efficiency when scanning from forward to reverse bias and an underestimation when scanning from reverse to forward bias.[33] We measure the steady-state values of the three critical points on the *J-V* curve: open circuit (V_{OC}), short circuit (J_{SC}), and the

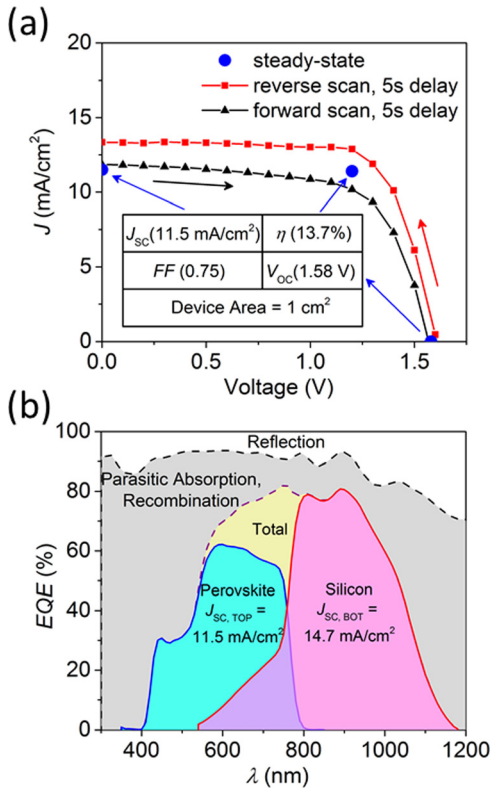

FIG. 3. (a) *J-V* curve of the 2-terminal perovskite/silicon multijunction solar cell under AM1.5G illumination. Forward and reverse-bias scan directions are shown with 5 s measurement delay per data point. Steady-state values for J_{SC}, V_{OC}, and MPP are measured by averaging over 30 s after reaching steady state. (b) Total device reflection and *EQE* of the perovskite and Si sub-cells of a typical perovskite/Si multijunction cell. The perovskite sub-cell *EQE* is corrected to match the measured J_{SC} and the silicon sub-cell *EQE* is reported as measured.[26]

maximum power point (MPP), depicted as blue circles (color online) in Figure 3(a) to negate hysteretic effects. The steady-state J_{SC} is 11.5 mA/cm^2, the steady-state V_{OC} is 1.58 V, and the steady-state MPP is 13.7% at 1.20 V bias (Figure S4).[26] These resultant fill factor (*FF*) is 0.75. The 1 cm^2 cell was aperture-masked to ensure a correct illumination area. The V_{OC} has been measured as high as 1.65 V in some devices. This result is encouraging, as the V_{OC} is approximately the sum of the V_{OC} for the perovskite top sub-cell and the bottom Si sub-cell illuminated through a separate semi-transparent perovskite device on FTO[9] (approximately 1.05 V and 0.55 V, respectively), further indicating proper operation of the tunnel junction.

The slow current-dynamics and corresponding hysteresis observed in the tandem resemble the sluggish dynamics of our perovskite solar cells and suggest that the perovskite sub-cell limits the current of the tandem.[33] This finding is substantiated by external quantum efficiency (*EQE*) measurements (Figure 3(b)) of the individual sub-cells.[26] Our tandem J_{SC} of 11.5 mA/cm^2 is low because the perovskite is illuminated through the *p*-type heterojunction, opposite from conventional perovskite devices. To understand the directional dependence of illumination on the perovskite sub-cell, we illuminate a semi-transparent single-junction perovskite solar cell[9] through the TiO_2 heterojunction and through the spiro-OMeTAD heterojunction. When illuminated through the TiO_2 heterojunction, the *EQE* of the semi-transparent cell integrates to 17.3 mA/cm^2, whereas when illuminated through the spiro-OMeTAD heterojunction the *EQE* integrates to 11.4 mA/cm^2 (Figure S5) due to low *EQE* for $\lambda < 550$ nm.[26] We attribute the lower photocurrent from the spiro-OMeTAD-side to parasitic absorption by the doped spiro-OMeTAD layer. From absorption measurements of doped spiro-OMeTAD on glass (Figure S6),[26] we estimate that the absorbed flux of the AM1.5G spectrum in this layer is 6.4 mA/cm^2 from 300–750 nm. We find that parasitic absorption by spiro-OMeTAD also reduces the photocurrent available to the bottom Si sub-cell, absorbing the equivalent of 2.0 mA/cm^2 of infrared photons from 750–1200 nm. The parasitic absorption can be reduced with a thinner spiro-OMeTAD layer, which is currently optimized to planarize a rough perovskite top surface to enable deposition of the silver nanowire electrode. With smoother perovskite films, the spiro-OMeTAD layer can achieve planarization with a thinner layer. The parasitic absorption may be completely removed by replacement of spiro-OMeTAD with an alternate *p*-type heterojunction contact that simultaneously exhibits both good conductivity and low parasitic absorption.

The perovskite sub-cell is also limited by quality of the perovskite absorber. Our single-junction perovskite cells with gold back contacts fabricated as control devices achieve at best 13.5% efficiency. Optimization of deposition conditions, precursor materials, and annealing protocols along with replacement or reduction of the spiro-OMeTAD layer is expected to yield a perovskite top sub-cell equivalent to the record single-junction perovskite cell, which currently stands at 20.1%.[3] For the Si sub-cell, applying a back-surface field and excellent surface passivation to the back of the bottom Si sub-cell, using dedicated furnaces, and decoupling the front surface passivation scheme from the tunnel junction formation are expected to yield improvements. We predict a Si sub-cell with a V_{OC} of 660–720 mV and a matched tandem J_{SC} of 18–19 mA/cm^2 when illuminated through the perovskite sub-cell. We expect, with these changes designed to improve the sub-cells to the match the highest quality devices available today, the monolithic tandem would have a V_{OC} of 1.84 V, a J_{SC} of 19 mA/cm^2, a *FF* of 0.83, and a corresponding efficiency of 29.0%. Ultimately, it has been suggested that perovskite/Si monolithic tandems can surpass 35% efficiency through careful photon management.[10]

In summary, we have demonstrated a 1 cm^2, 2-terminal monolithically-integrated metal-halide perovskite/Si multijunction solar cell. The monolithic integration is enabled by a Si-based tunnel junction fabricated directly on top of the bottom Si sub-cell emitter and by incorporating a semi-transparent silver nanowire-based top electrode. We obtained a multijunction device V_{OC} as high as 1.65 V, which is the expected sum of the perovskite and filtered Si V_{OC}'s, demonstrating the potential of this approach. The best 2-terminal multijunction prototype device efficiency is 13.7% and is current-limited by the perovskite sub-cell. This value is low compared to the record efficiency for perovskite or Si cells, in part because this tandem prototype does not yet have best-in-class perovskite and Si layers. Further improvements can be achieved by replacing the spiro-OMeTAD layer with wider band gap hole transport material, improving the

quality of the perovskite absorber, use of dedicated furnaces for the Si sub-cell fabrication, and by implementing better surface passivation schemes on the front and back side of the Si sub-cell. These improvements can yield a 29.0% efficient tandem, with the ultimate efficiency potential of these monolithic tandems surpassing 35%.

H. Wagner, J. Z. Lee, S. C. Siah, and S. E. Sofia (MIT) are thanked for silicon cell design advice. Y. S. Lee (MIT), A. Scheuermann (Stanford), and M. Hathaway (Harvard CNS) are thanked for ALD TiO_2 deposition advice. Z. K. Ren, N. S. Khanghah, I. M. Peters (SMART), H. Liu, Z. Liu, L. Fen (SERIS), R. Jones-Albertus (DOE) and S. A. Ringel (Ohio State University) are thanked for helpful discussions. This work was supported by Bay Area Photovoltaic Consortium (BAPVC) under Contract No. DE-EE0004946, and the U.S. Department of Energy (DOE) under Contract No. DE-EE0006707. This work was performed in part at the Center for Nanoscale Systems (CNS), a member of the National Nanotechnology Infrastructure Network (NNIN), which is supported by the National Science Foundation under NSF award no. ECS-0335765.

[1]P. A. Basore, IEEE J. Photovoltaics **4**, 1477 (2014).
[2]D. M. Powell, M. T. Winkler, A. Goodrich, and T. Buonassisi, IEEE J. Photovoltaics **3**, 662 (2013).
[3]M. A. Green, K. Emery, Y. Hishikawa, W. Warta, and E. D. Dunlop, Prog. Photovoltaics Res. Appl. **23**, 1 (2015).
[4]K. Masuko, M. Shigematsu, T. Hashiguchi, D. Fujishima, M. Kai, N. Yoshimura, T. Yamaguchi, Y. Ichihashi, T. Mishima, N. Matsubara, T. Yamanishi, T. Takahama, M. Taguchi, E. Maruyama, and S. Okamoto, IEEE J. Photovoltaics **4**, 1433 (2014).
[5]R. M. Swanson, in Proceedings of 31st IEEE Photovoltaic Specialist Conference (2005), Vol. 889.
[6]M. Umeno, T. Soga, K. Baskar, and T. Jimbo, Sol. Energy Mater. Sol. Cells **50**, 203 (1998).
[7]K. Tanabe, K. Watanabe, and Y. Arakawa, Sci. Rep. **2**, 349 (2012).
[8]Z. M. Beiley and M. D. McGehee, Energy Environ. Sci. **5**, 9173 (2012).
[9]C. D. Bailie, M. G. Christoforo, J. P. Mailoa, A. R. Bowring, E. L. Unger, W. H. Nguyen, J. Burschka, N. Pellet, J. Z. Lee, M. Grätzel, R. Noufi, T. Buonassisi, A. Salleo, and M. D. McGehee, Energy Environ. Sci. **8**, 956 (2015).
[10]P. Loper, B. Niesen, S.-J. Moon, S. Martin de Nicolas, J. Holovsky, Z. Remes, M. Ledinsky, F.-J. Haug, J.-H. Yum, S. De Wolf, and C. Ballif, IEEE J. Photovoltaics **4**, 1545 (2014).
[11]F. Meillaud, A. Shah, C. Droz, E. Vallat-Sauvain, and C. Miazza, Sol. Energy Mater. Sol. Cells **90**, 2952 (2006).
[12]M. Liu, M. B. Johnston, and H. J. Snaith, Nature **501**, 395 (2013).
[13]M. M. Lee, J. Teuscher, T. Miyasaka, T. N. Murakami, and H. J. Snaith, Science **338**, 643 (2012).
[14]J.-H. Im, C.-R. Lee, J.-W. Lee, S.-W. Park, and N.-G. Park, Nanoscale **3**, 4088 (2011).
[15]J. Burschka, N. Pellet, S.-J. Moon, R. Humphry-Baker, P. Gao, M. K. Nazeeruddin, and M. Grätzel, Nature **499**, 316 (2013).
[16]N. J. Jeon, J. H. Noh, W. S. Yang, Y. C. Kim, S. Ryu, J. Seo, and S. Il Seok, Nature **517**, 476 (2015).
[17]A. Ishii, A. K. Jena, and T. Miyasaka, APL Mater. **2**, 091102 (2014).
[18]J. H. Noh, S. H. Im, J. H. Heo, T. N. Mandal, and S. Il Seok, Nano Lett. **13**, 1764 (2013).
[19]E. T. Hoke, D. J. Slotcavage, E. R. Dohner, A. R. Bowring, H. I. Karunadasa, and M. D. McGehee, Chem. Sci. **6**, 613 (2015).
[20]P. Löper, S.-J. Moon, S. Martín de Nicolas, B. Niesen, M. Ledinsky, S. Nicolay, J. Bailat, J.-H. Yum, S. De Wolf, and C. Ballif, Phys. Chem. Chem. Phys. **17**, 1619 (2015).
[21]L. Esaki, Phys. Rev. **109**, 603 (1958).
[22]T. Todorov, T. Gershon, O. Gunawan, C. Sturdevant, and S. Guha, Appl. Phys. Lett. **105**, 173902 (2014).
[23]G. J. Bauhuis, P. Mulder, and J. J. Schermer, Prog. Photovoltaics Res. Appl. **22**, 656 (2014).
[24]F. A. Rubinelli, J. K. Rath, and R. E. I. Schropp, J. Appl. Phys. **89**, 4010 (2001).
[25]K. Tvingstedt, O. Malinkiewicz, A. Baumann, C. Deibel, H. J. Snaith, V. Dyakonov, and H. J. Bolink, Sci. Rep. **4**, 6071 (2014).
[26]See Supplementary Material at http://dx.doi.org/10.1063/1.4914179 for fabrication and characterization details.
[27]Y. Wang, X. Liao, Z. Ma, G. Yue, H. Diao, J. He, G. Kong, Y. Zhao, Z. Li, and F. Yun, Appl. Surf. Sci. **135**, 205 (1998).
[28]N. Jin, S. Chung, A. T. Rice, P. R. Berger, P. E. Thompson, C. Rivas, R. Lake, S. Sudirgo, J. J. Kempisty, B. Curanovic, S. L. Rommel, K. D. Hirschman, S. K. Kurinec, P. H. Chi, and D. S. Simons, IEEE Trans. Electron Devices **50**, 1876 (2003).
[29]D. Gebeyehu, C. J. Brabec, N. S. Sariciftci, D. Vangeneugden, and R. Kiebooms, Synth. Met. **125**, 279 (2001).
[30]S. Avasthi, W. E. McClain, G. Man, A. Kahn, J. Schwartz, and J. C. Sturm, Appl. Phys. Lett. **102**, 203901 (2013).
[31]J. Jhaveri, S. Avasthi, K. Nagamatsu, and J. C. Sturm, in Proceedings of 40th IEEE Photovoltaic Specialist Conference (2014), Vol. 1525.
[32]W. H. Nguyen, C. D. Bailie, E. L. Unger, and M. D. McGehee, J. Am. Chem. Soc. **136**, 10996 (2014).
[33]E. L. Unger, E. T. Hoke, C. D. Bailie, W. H. Nguyen, A. R. Bowring, T. Heumuller, M. G. Christoforo, and M. D. McGehee, Energy Environ. Sci. **7**, 3690 (2014).